Mesoporous Carbon−Vanadium Oxide Films by Resol-Assisted, Triblock Copolymer-Templated Cooperative Self-Assembly

Sarang M. Bhaway,[†] Kim Kisslinger,[‡] Lihua Zhang,[‡] Kevin G. Yager,[‡] Andrew L. Schmitt,[§] Mahesh K. Mahanthappa,[§] Alamgir Karim,[†] and Bryan D. Vogt*,[†]

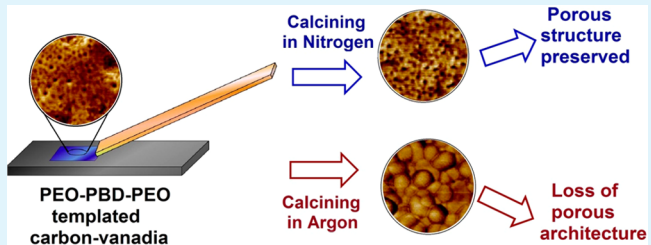[†]Department of Polymer Engineering, University of Akron, Akron, Ohio 44325, United States
[‡]Center for Functional Nanomaterials, Brookhaven National Laboratory, Upton, New York 11973, United States
[§]Department of Chemistry, University of Wisconsin−Madison, Madison, Wisconsin 53706, United States

Ⓢ Supporting Information

ABSTRACT: Unlike other crystalline metal oxides amenable to templating by the combined assemblies of soft and hard chemistries (CASH) method, vanadium oxide nanostructures templated by poly(ethylene oxide-*b*-1,4-butadiene-*b*-ethylene oxide) (OBO) triblock copolymers are not preserved upon high temperature calcination in argon. Triconstituent cooperative assembly of a phenolic resin oligomer (resol) and an OBO triblock in a $VOCl_3$ precursor solution enhances the carbon yield and can prevent breakout crystallization of the vanadia during calcination. However, the calcination environment significantly influences the observed mesoporous morphology in these composite thin films. Use of an argon atmosphere in this processing protocol leads to nearly complete loss of carbon−vanadium oxide thin film mesostructure, due to carbothermal reduction of vanadium oxide. This reduction mechanism also explains why the CASH method is not more generally successful for the fabrication of ordered mesoporous vanadia. Carbonization under a nitrogen atmosphere at temperatures up to 800 °C instead enables formation of a block copolymer-templated mesoporous structure, which apparently stems from the formation of a minor fraction of a stabilizing vanadium oxynitride. Thus, judicious selection of the inert gas for template removal is critical for the synthesis of well-defined, mesoporous vanadia−carbon composite films. This resol-assisted assembly method may generally apply to the fabrication of other mesoporous materials, wherein inorganic framework crystallization is problematic due to kinetically competitive carbothermal reduction processes.

KEYWORDS: block copolymer, self-assembly, vanadia, templated synthesis, nanopores, FDU-16

■ INTRODUCTION

Significant efforts[1−3] have increased the chemical diversity[4] of soft-templated, ordered mesoporous materials, since the original report of the Mobil composition of matter (MCM)[5] family of silicate materials. However, the scalable synthesis of well-defined mesoporous materials with highly crystalline frameworks under high temperature processing conditions remains challenging.[6] Commercially available organic templates, such as Pluronic poly(ether) triblock copolymers, generally decompose prior to significant inorganic framework crystallization, leading to losses in templated porosity as the crystals break out and grow through the pores.[7] Thus, most frameworks in mesoporous materials are at best semicrystalline with numerous grain boundaries,[4,8,9] which limits their electronic and electrochemical applications.[10] Hard templating[11] by mesoporous silica[12] or carbon[13] provides a means of increasing crystallite size and overall crystallinity, yet the increased time and costs associated with template synthesis and its postprocessing removal render this method inefficient. The poorly crystalline framework of a mesoporous material may be alternatively coated with carbon and silica for elevated temperature crystallization without loss of porosity, again at increased time and expense.[14]

Wiesner and co-workers pioneered the combined assemblies of soft and hard chemistries (CASH) methodology for mesoporous metal oxide synthesis, in which inorganic framework crystallization breakout into the mesopores is physically prevented by carbon derived from the block copolymer template.[15] Thus, the CASH method enables the synthesis of a broad variety of mesoporous transition metal oxides.[16] For example, a titania sol templated by a poly(isoprene-*b*-ethylene oxide) (PI-*b*-PEO) copolymer was calcined under argon to effectively crystallize TiO_2 with the mesostructure protected during crystallization by carbon generated in situ from the PI segment of the template.[15] Calcination under air instead led to loss of porosity due to full degradation of the block copolymer and subsequent titania sintering.[7] In spite of these advances afforded by the CASH method, most reports of ordered

mesoporous metal oxides with highly crystallizable frameworks have focused on low temperature calcination/crystallization[17] or alternative processing techniques, such as microwave-assisted synthesis[18] and the addition of nucleation aids,[19] to mitigate loss of porosity by breakout crystallization.

Ideally, the CASH method[20] should furnish a robust route for generating thin carbon coatings on the desired framework chemistry to generate well-defined metal oxide−carbon composites. These metal oxide−carbon composites are particularly promising for electrical energy storage applications.[21−24] For example, introduction of low concentrations of vanadia (<20 wt %) into mesoporous carbon dramatically increases its supercapacitor performance.[24] Vanadium oxide electrodes also exhibit low electrical conductivities[25] and poor cycling stabilities,[26] which may be ameliorated by the formation of carbon−vanadia composite electrodes.

The transformation of soft-templated vanadia[27,28] into an ordered mesoporous structure is challenging due to the low temperature crystallization of vanadium oxide at ∼250 °C under an inert atmosphere.[29] A rapid calcination protocol can overcome this limitation to retain the mesoporous vanadia structure using a poly(ethylene oxide-b-polystyrene) (PS-b-PEO) template that yields large pore sizes (30−35 nm).[30] More recently, multicomponent mixtures comprising a metal oxide sol, a block copolymer template, and the carbonizable precursor resol[31] provide a route to fabricate high porosity mesoporous materials of easily crystallizable metal oxides even upon elevated temperature processing. In this case, the resol provides carbon yield in the framework, not just at the interface with the template as in the standard CASH method. However, access to ordered mesoporous materials with significantly higher concentrations of vanadium oxide poses the significant challenge of maintaining porosity upon template removal.[9,29] For example, addition of vanadium oxide in excess of 35 wt % induces partial macrophase separation of the inorganic components from the block copolymer template.[32]

Herein, to attempt to address these limitations, we examine the efficacy of the CASH method for generating mesoporous carbon−vanadia composite films using vanadium(V) oxychloride and poly(ethylene oxide-b-1,4-butadiene-b-ethylene oxide) (OBO) triblock copolymer as the template, whereby the B segment provides the carbon yield requisite for CASH. As an alternative, the triconstituent cooperative assembly of an OBO triblock with both resol and VOCl₃ is shown to significantly increase the carbon content in the final product, simply by tuning of the VOCl₃:resol ratio in the precursor solution (as a resol-assisted CASH method). We find that preservation of the templated mesostructure during elevated temperature calcination sensitively depends on the judicious choice of calcining environment: nitrogen or argon. Calcination under nitrogen leads to the greatest mesostructure retention upon inclusion of resol in the synthesis, whereas argon leads to a complete loss of the templated mesostructure at high temperatures. Through structural, chemical, and thermal analyses of the films, we show that this calcination environment-dependent morphology difference stems from the ready carbothermal reduction of the vanadia in argon. Under a nitrogen atmosphere, vanadia carbothermal reduction is apparently inhibited by the formation of a small fraction of a vanadium oxynitride that leads to mesostructure retention even upon heating to 800 °C. This mesoporous morphology significantly improves the electrochemical capacitance of the resulting vanadium oxide−carbon composite in NaSO₄(aq) at high rates, as determined by cyclic

voltammetry. Thus, resol-assisted assembly of the vanadium oxide preserves the block copolymer-templated mesostructure at elevated temperatures in a manner unachievable with the CASH method alone.

■ EXPERIMENTAL SECTION

Materials. Phenol (>99%), formaldehyde (ACS reagent, 37 wt % (aq) with 10−15% methanol stabilizer), NaOH (ACS reagent, > 97%), conc. hydrochloric acid (ACS reagent, 37 wt % (aq)), vanadium(V) oxychloride (99%), and 2-butanol (ACS reagent, > 99%) were purchased from Sigma-Aldrich and used as received. Chloroform (technical grade, 0.75% ethanol preservative) was purchased from Fisher Scientific.

To template the mesostructure, poly(ethylene oxide-b-1,4-butadiene-b-ethylene oxide) (OBO) triblock copolymer with M_n = 16 kg/mol and f_{PEO} = 0.36 was used. The synthesis of this block copolymer was previously reported.[33] Although this block copolymer has a broader dispersity, Đ = M_w/M_n = 1.46, than typical copolymer templates, this material generates a well-defined nanoscale morphology. We note that broad copolymer dispersity results in increased domain sizes for the center B block, even at low molecular weights.[34]

For the carbonizable precursor, phenol and formaldehyde were condensed using NaOH to form a low molecular weight, thermally cross-linkable resol phenolic resin as described previously.[35] The reaction mixture was neutralized using 1 M HCl(aq) to pH ∼7. Water was removed from the synthesized resol by rotary evaporation at 46 °C under vacuum. The resulting liquid resol was dissolved in 2-butanol to yield a 20 wt % solution, and any precipitated NaCl(s) was removed from the solution using a 0.45 μm glass filter.

Silicon wafers (Silicon, Inc.) were used as substrates and were cleaned using ultraviolet (UV) ozone (Jelight, model no. 42) for 1 h prior to use. Two different silicon wafers were used, depending on the experiment. For Fourier transform infrared (FTIR) measurements, high resistivity (>10 Ω·cm), 500 μm thick double side polished Si wafers were used, whereas cyclic voltammetry measurements employed highly conductive 600 μm thick silicon wafers (resistivity = 0.01−0.02 Ω·cm).

Sample Preparation. Films were prepared by first dissolving 20 mg of OBO triblock copolymer in 2 mL of CHCl₃ at 22 °C. For the CASH method, 75 mg of VOCl₃ was added slowly to 0.15 g of 2-butanol and the mixture was stirred for 10 min, after which 2 mL of CHCl₃ solution containing 20 mg of OBO copolymer was passed through a 0.45 μm glass filter and added to the vanadia sol. After the sol−gel solution was aged for 1 h, thin films were cast by flow coating[36] at 40 mm/s and a relative humidity of ∼30−40%. For resol-assisted assembly, 20 mg of VOCl₃ was added slowly to 0.2 g of 20 wt % resol in 2-butanol and the mixture was stirred for 10 min in a separate vial. After 10 min, 2 mL of CHCl₃ solution containing 20 mg of OBO copolymer was passed through a 0.45 μm glass filter and added to the resol−vanadia sol. The final mass ratios of the solids, resol:VOCl₃:OBO copolymer was fixed at 2:1:1 for all films shown here. This solution was subjected to continuous vigorous stirring for 1 h at 22 °C prior to film casting. Thin films were then immediately cast from the solution by flow coating[36] at 40 mm/s and a relative humidity of ∼30−40%.

All coated films were allowed to age for 10−12 h at ambient temperature and humidity (∼30−40% RH). Subsequently, all the films were heated at 120 °C for 24 h. The purpose of this heating is to cross-link the resol following prior protocols,[35] but all films irrespective of resol content were processed identically for consistency. The template was removed by calcination in a tube furnace (SentroTech Corp.) with a gas purge of either nitrogen (Praxair, Industrial grade, [O₂] < 5 ppm) or argon (Praxair, grade AR5.0 UH, [O₂] < 1 ppm) at 100 mL/min. The heating schedule for template removal was an initial ramp to 350 °C at 1 °C/min and a 2 h hold at 350 °C, followed by heating at 1 °C/min to the final target temperature with an additional 1 h hold at that temperature. Samples were then cooled to ambient temperature at 1 °C/min. Three different target temperatures were used to fabricate mesoporous polymer−vanadium oxide (450 °C) or carbon−vanadium

oxide thin films (600 or 800 °C). We use the sample nomenclature "CV-*x*-*y*", where CV denotes the carbon–vanadia composite, *x* denotes the target temperature and *y* represents the gas environment used: nitrogen (N_2) or argon (Ar). For thin films cast following the CASH method without any resol, an analogous heating protocol in an Ar environment was employed. These thin films are named as CASH-*x*-Ar, using the previously described convention.

Characterization. Spectroscopic ellipsometry (M-2000, J.A. Woollam) was used to elucidate the thickness and refractive index of the films after each processing step. Ellipsometric porosimetry (EP) was used to assess the porosity and pore size distribution of the composite thin films. Toluene was used as the probe solvent for EP. The change in refractive index as a function of the partial pressure of toluene was monitored by in situ ellipsometry, where the sample is contained in a cell with quartz windows at 70° relative to the normal vector to the film surface. The pore size distribution was estimated using the Kelvin equation for the adsorption isotherm.[37] The surface morphology was also investigated at each step (as cast, thermopolymerized, and calcined) using atomic force microscopy (AFM, Dimension ICON, Veeco). Grazing incidence small-angle X-ray scattering (GISAXS) was performed at the 8-ID-E beamline at the Advanced Photon Source (APS) of Argonne National Laboratory and the X9 beamline of National Synchrotron Light Source (NSLS) at Brookhaven National Laboratory (BNL). At APS, the films were illuminated with 7.35 keV radiation at incident angles (α_i) of 0.1°–0.2° under vacuum; the off-specular scattering was recorded with a Pilatus 1MF pixel array detector (pixel size = 172 μm) with a sample-to-detector distance of 2175 mm. At NSLS, an incident X-ray beam energy of 13.5 keV was used and scattering data were collected using a charged-coupled device (CCD) detector at a distance of 4.73 m. All samples under vacuum ($\approx$40 Pa) were measured at multiple angles both below and above the critical angle. The crystal structures of the films were assessed with grazing incidence X-ray diffraction (GIXD). GIXD was carried out at NSLS using incident X-ray energy of 13.5 keV and the scattering data were collected on a CCD detector. Complementary real space images were obtained by transmission electron microscopy (TEM) using a JEOL JEM2100F microscope in both bright- and dark-field imaging modes. The TEM samples were prepared using the focused ion beam (FIB) in situ lift-out specimen technique.[38] Additionally, nitrogen calcined films were scrapped off from the silicon wafer and pulverized into fine powder. The powdered sample was dispersed in ethanol solvent and subjected to ultra-sonication, followed by transferring onto a carbon coated copper grid. Transmission electron microscopy (TEM) was performed on a Tecnai G2 20S-TWIN apparatus at an accelerating voltage of 200 kV.

To investigate the carbon and vanadium oxide contents in the calcined composites, we performed thermogravimetric analysis (TGA) on crushed powders of resol and vanadium oxide composites. Crushed powders were prepared by first forming a sol of resol and $VOCl_3$, having the same initial composition as that used for casting thin films; the only difference being the absence of the OBO block copolymer template in the sol. This sol was poured into a dish and the solvent was allowed to evaporate at 22 °C for 8–10 h, followed by thermopolymerization of resol at 120 °C for 24 h. Thermogravimetric analysis (TGA, TA Instruments, TGA-Q50) was performed on these thermopolymerized resol–vanadia powders with either nitrogen or argon purge over a temperature range of 22–800 °C. The heating schedule (rate and hold) for these TGA measurements was identical to that used for the fabrication of the films described previously. These carbonized powders were subsequently analyzed with an air purge to determine the vanadium oxide content of the materials after carbonization at a heating rate of 10 °C/min.

To assess the chemical composition of the calcined composite thin films, X-ray photoelectron spectroscopy (XPS, PHI 5000 Versa probe II scanning XPS microprobe, ULVAC-PHI, Inc.) with high resolution scans at energies associated with C 1s, O 1s, and V 2p was performed using a 0.05 eV step size and a pass energy of 11.75 eV. The scans were recorded at a takeoff angle of 45°, probing approximately 10 nm into the surface of the thin films. The peaks associated with V 2p were deconvoluted using peak fitting (IGOR Pro, Wavemetrics) in order to

determine the oxidation states of vanadium in the films. Additionally, FTIR spectra (Thermo Scientific, Nicolet iS50 FT-IR) were obtained in transmission mode on the thin films using 256 scans with a resolution of 4 cm^{-1} using a deuterated triglycine sulfate (DTGS) detector. Spectra were baseline corrected using the OMNIC software.

The electrical conductivity of the carbon–vanadium oxide thin films was determined by four-point probe measurement (Pro-4, Lucas Labs) with a Keithley Series 2400 SourceMeter. The spacing between the pins on the probe head was 0.04 in. The electrical conductivity was corrected for the film thickness using typical geometric arguments.[39] To assess the electrochemical capacitance of the films, cyclic voltammetry using a three-electrode cell with Pt wire as the counter electrode and Ag/AgCl as the reference electrode was performed with a CHI630 electrochemical analyzer (CH Instruments). The cyclic voltammetry experiments used 1 M Na_2SO_4(aq) as the electrolyte at ambient temperature and the impact of scan rate (2–100 mV/s) on charge storage was investigated. The apparent capacity of the CV-800-N_2 film was compared to the capacity of a nontemplated, nonporous film prepared using identical processing conditions without the OBO triblock.

■ RESULTS AND DISCUSSION

Figure 1 illustrates the change in the surface morphology of films at various stages of the fabrication process following the
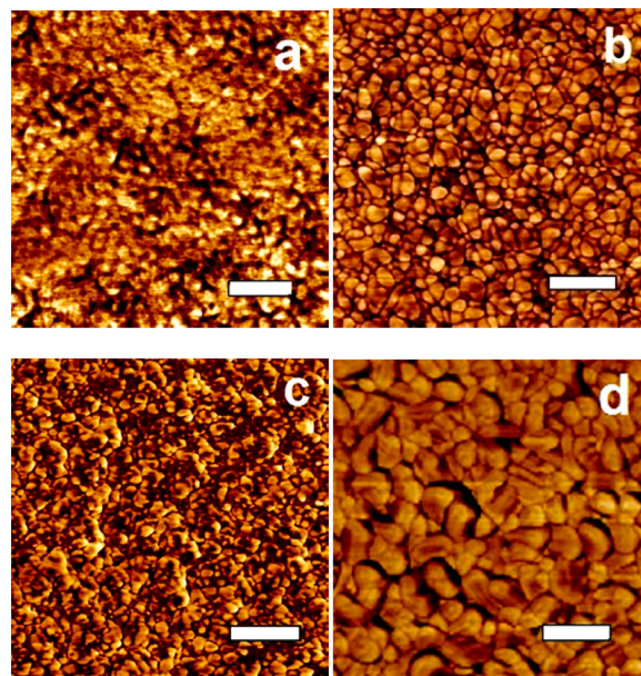
Figure 1. AFM phase images of OBO triblock-templated polymer–vanadia thin film (a) as cast, and after calcination in (b) Ar (CASH-450-Ar), (c) N_2 (CASH-450-N_2), and (d) in air at 450 °C. The mesostructure in the as-cast composite film is not preserved upon template removal, irrespective of calcining environment (scale bar = 200 nm).

CASH protocol (without any addition of resol).[15] Initially, the OBO triblock leads to poorly defined micelles templated into the vanadia composite (Figure 1a). The templated structure lacks any long-range order, yet a common length scale of ~24 nm associated with the microphase separation of the OBO template is observed in the as-cast films. Calcination in an argon environment per the standard CASH protocol[15] leads to loss of this nanostructure at 450 °C (CASH-450-Ar), as shown in Figure 1b. This CASH protocol leads to formation of large

vanadia crystals that are approximately 60–75 nm across, which are significantly larger than those in the original templated structure. This loss of the templated morphology suggests that the CASH method is incapable of preventing breakout crystallization in this system.

OBO triblock-templated vanadia thin films instead calcined under $N_2(g)$ at 450 °C exhibited a similar loss of mesostructure (Figure 1c). The thermal stability of the OBO template in Ar and N_2 environments is found to be similar, with a degradation onset temperature of approximately 400 °C (Figure S1 in the Supporting Information). In spite of the similar degradation behaviors of the OBO template under both Ar and N_2, the size of the evolved vanadia crystals on the surface is significantly smaller using N_2 (35–50 nm) as opposed to Ar (60–75 nm). Moreover, direct calcination in air leads to significantly larger crystals at the same processing conditions (Figure 1d), implying that there is some suppression in the crystal growth in the "inert" atmospheres with the N_2 being surprisingly more effective. Nonetheless, the structure templated by the OBO triblock is lost in all cases of calcination at 450 °C, even when following the CASH protocol.[15]

Previous work has demonstrated similar losses of surfactant-templated mesostructure on calcinination of vanadia-based systems.[9] This destruction of the mesostructure on template removal is attributed to the low temperature crystallization of vanadium oxide and the associated breakout crystallization that is accompanied by collapse of the porous mesostructure.[9,29] However, the CASH method[15] is designed to prevent this crystallization breakout through in situ carbon generation ("carbon yield") that leads to hard templating of the metal oxide component.[16] The failure of CASH under these circumstances suggests that the carbon yield is insufficient for effective templating.

Therefore, we reasoned that introduction of an additional component that would enhance the carbon yield upon thermal treatment in the CASH process might enable more effective hard templating to produce mesoporous vanadia films. Consequently, we devised a resol-assisted multicomponent assembly, wherein resol serves as a precursor that enhances the carbon yield to provide a more effective template. Thermally polymerized resol, a resin derived from phenol and formaldehyde, on its own can provide up to 58 wt % carbon upon heating at 800 °C, as shown in Figure S1 (Supporting Information). The mesoporous structure shown in the AFM image in Figure 2 arose from the triconstituent thin film composites of OBO triblock template, resol, and vanadia. Unlike the previous samples lacking resol (Figure 1), removal of the template by calcination at 450 °C under N_2 (CV-450-N_2, Figure 2a) or Ar (CV-450-Ar, Figure 2b) leads to a mesostructured porous film that retains the triblock copolymer-templated structure. This result suggests that the additional carbon yield from the resol prevents the breakout crystallization as the structure is lost on calcination in air (see Figure S2, Supporting Information), whereby resol pyrolysis to oxidized gases occurs. The hydrophobic nature of the poly(1,4-butadiene) segment in the OBO copolymer ideally promotes formation of spherical micelles in chloroform. These micelles tend to pack in a cubic (BCC) mesostructure when the concentration of the BCP is increased.[40] The spherical features observed in Figure 2 are consistent with this expected cubic mesostructure. Note that block copolymer-templated vanadium oxide calcined in argon at 400 °C appears porous under these conditions, thus it appears possible to maintain some porosity
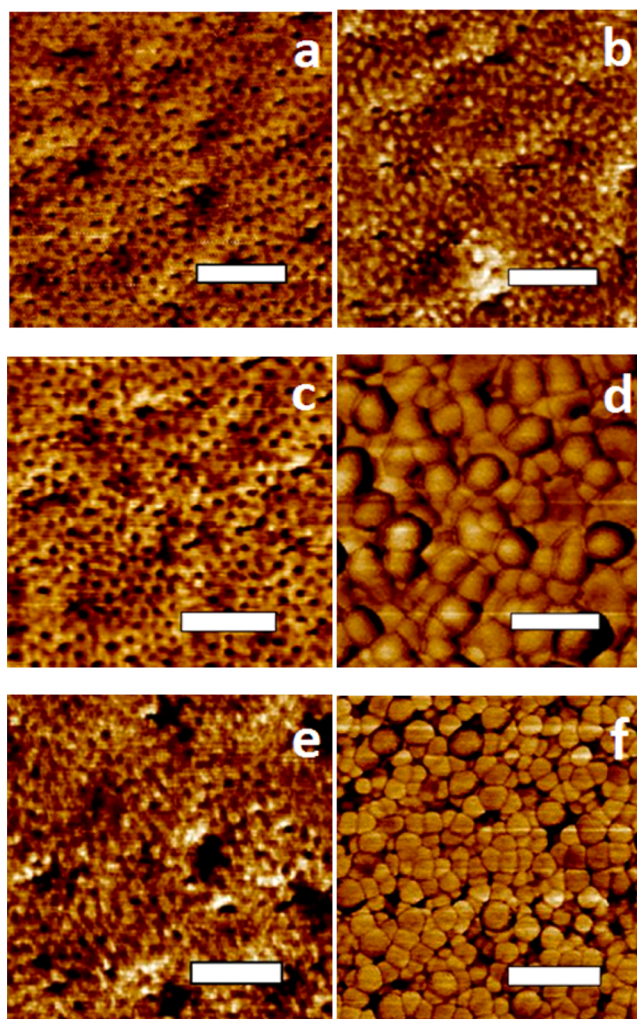
Figure 2. AFM phase images of resol-assisted triconstituent thin films of (a) CV-450-N_2, (b) CV-450-Ar, (c) CV-600-N_2, (d) CV-600-Ar, (e) CV-800-N_2, and (f) CV-800-Ar. The templated mesoporous carbon–vanadium oxide morphology is partially preserved after calcination under N_2 (scale bar = 200 nm).

without resol by careful control of the calcination conditions.[41] However, the addition of resol appears to provide a more facile and tolerant approach to robust mesoporous structures containing vanadium oxide. An important point to note is that the $VOCl_3$ concentration in the precursor is crucial to obtain an ordered porous structure. Higher loadings of $VOCl_3$ led to a loss of the ordered mesostructure on heating and template removal at 450 °C.

For the porous films reported thus far, the resol remains polymeric and thus nonconducting upon heating to 450 °C.[35] Increasing the calcination temperature to 600 °C, at which the resol becomes carbonaceous, markedly transforms the observed morphology, depending on the calcination atmosphere. When calcined in N_2 at 600 °C, mesoscale order remains after resol carbonization (CV-600-N_2, Figure 2c). The average pore diameter decreases slightly from 22.5 to 20 nm based on AFM images, as the calcination temperature is increased from 450 to 600 °C, respectively. Similarly, the average d-spacing estimated from the fast Fourier transform (FFT) of the AFM micrographs indicates a 9.2% decrease in the d-spacing from 32.8 nm for CV-450-N_2 to 29.8 nm for CV-600-N_2. However, calcination under Ar at 600 °C destroys the templated structure
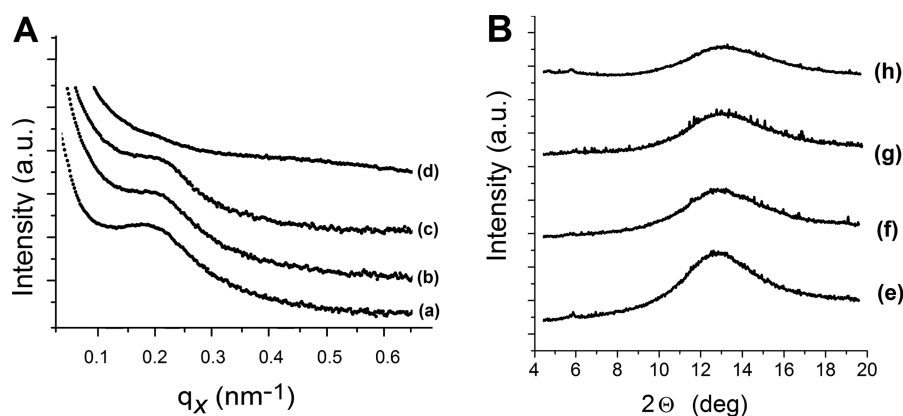
Figure 3. (A) 1D plots extracted from the in-plane direction of GISAXS patterns at $\alpha = 0.2°$ (above critical angle) for (a) CV-450-Ar, (b) CV-450-N$_2$, (c) CV-600-N$_2$, and (d) CV-800-N$_2$. (B) Comparison of GIXD 1D profiles for (e) CV-600-N$_2$, (f) CV-600-Ar, (g) CV-800-N$_2$, and (h) CV-800-Ar.

(CV-600-Ar, Figure 2d), due to formation of large vanadia crystals (∼60−75 nm in size). Further increasing the calcination temperature to 800 °C under N$_2$ worsens the mesoscale ordering (CV-800-N$_2$, Figure 2e), with only partial preservation of the copolymer-templated structure. As expected, breakout crystallization occurs in Ar at this same temperature (CV-800-Ar, Figure 2f). Both morphologies arising from breakout crystallization (CV-600-Ar and CV-800-Ar) appear similar to the mesostructure obtained using CASH-450-Ar. Thus, the presence of carbon alone is not sufficient to preserve a porous architecture and the inert calcining environment plays a crucial role in this regard.

To confirm that the surface features observed by AFM reflect the bulk morphology of the thin film, we conducted grazing-incidence small-angle X-ray scattering (GISAXS) on the templated thin films. As shown in Figure 3, a single, broad scattering peak associated with the in-plane correlation of the mesoporous structure is observed in 1D $I(q)$ vs q plots extracted from the 2D GISAXS images. Because the angle of the incident X-ray beam (0.2°) is greater than the critical angle of vanadium oxide,[42] these measurements probe the entire depth of the composite film to provide an average correlation length therein. The absence of higher order Bragg peaks in the scattering data is not unexpected, based on the short-range translational order observed by AFM. The broad primary peak at $q_x \approx 0.188$ nm^{-1} for CV-450-Ar (Figure 3a) corresponds to a d-spacing of 33.4 nm, whereas scattering from CV-450-N$_2$ (Figure 3b) exhibits a similar broad peak in the in-plane direction at $q_x \approx 0.19$ nm^{-1} ($d = 33.1$ nm). This comparative scattering analysis of CV-450-Ar and CV-450-N$_2$ agrees well with the similar short-range ordered porous polymer−vanadium oxide thin films determined from the AFM micrographs (Figure 2a,b). The similarities in these scattering features indicate that the calcination environment (N$_2$ or Ar) does not significantly impact the ordering length scale of the mesoporous polymer−vanadium oxide structure at 450 °C.

As the calcination temperature is increased to 600 °C, the scattering peak shifts to a higher $q_x = 0.212$ nm^{-1} for CV-600-N$_2$ (Figure 3c), corresponding to a decrease in the d-spacing to 29.6 nm from 33.1 nm at 450 °C. These results agree well with the characteristic length scales calculated from the FFT of the AFM micrographs (Figure 2) as the spacing decreases from 32.8 nm for CV-450-N$_2$ to 29.8 nm for CV-600-N$_2$. We ascribe this d-spacing decrease to shrinkage of pores and contraction of

the composite carbon−vanadium oxide thin film on calcination. It is interesting that the in-plane d-spacing decreases during this processing, as uniaxial contraction is typically observed for templated mesoporous thin films of silica,[43] other metal oxides,[40] and carbon.[44] We can compare this contraction in the in-plane d-spacing to the contraction in the film thickness, which typically is well correlated with the changes in the out-of-plane d-spacing (this cannot be determined as these out-of-plane diffraction peaks are weak and thus hidden by the beamstop in these GISAXS measurements). The film contraction for CV-450-N$_2$ from ellipsometric measurements is 53% in comparison to the as-cast film (330 nm), whereas the film of CV-600-N$_2$ exhibits 64% contraction (Figure S3, Supporting Information). Between 450 and 600 °C, there is a 10% decrease in the in-plane d-spacing, while the film thickness decreases by 23%. Thus, there is a preferred contraction of the film through its thickness, but there is still a substantial decrease of the in-plane dimension. This analysis suggests that the structure of these templated resol−vanadia composite films continue to evolve during thermal processing.

For CV-800-N$_2$ composite films, only a single, very weak and broad scattering peak is observed (Figure 3d). To estimate the peak position, the 1D scattering profile was fit with a combination of an exponential decay (to describe the background scattering) and a Lorentzian function (Figure S4 in the Supporting Information). From this procedure, the d-spacing is estimated to be 30.8 nm for CV-800-N$_2$. This weak scattering signature is consistent with the poor short-range ordering observed by AFM for CV-800-N$_2$. It should be noted that no significant scattering, outside of the background associated with a nontemplated film, is obtained for CV-600-Ar and CV-800-Ar due to loss of the self-assembled mesostructure on calcination.

To further understand how processing impacts the evolution of vanadia crystal structure, Figure 3B illustrates the grazing incidence X-ray diffraction (GIXD) for these films. All calcined films exhibit a broad diffraction peak at $2\theta \sim 12.8°$, which corresponds to the (002) reflection of amorphous carbon.[35] Metal oxides are known to promote partial graphitization upon heating in excess of 750 °C.[45] However, the broad carbon peak indicates that limited graphitization for these carbon−vanadia composites, even after heating to 800 °C. No clear diffraction peaks associated with vanadia are visible in the spectrum. This

implies that the vanadia is either amorphous or the crystallite size is extremely small for these mesoporous composites in N_2.

To further analyze the nanoporous morphology of these carbon−vanadium oxide composites, cross-sectional TEM micrographs were obtained for the calcined thin films to elucidate the lateral structure through the thickness of the film. After calcination at 600 °C, CV-600-N_2 exhibits asymmetric ellipsoidal pores with their semimajor axes (22 ± 4 nm) oriented parallel to the silicon substrate, as shown in the bright-field micrograph in Figure 4a. This long-axis dimension is
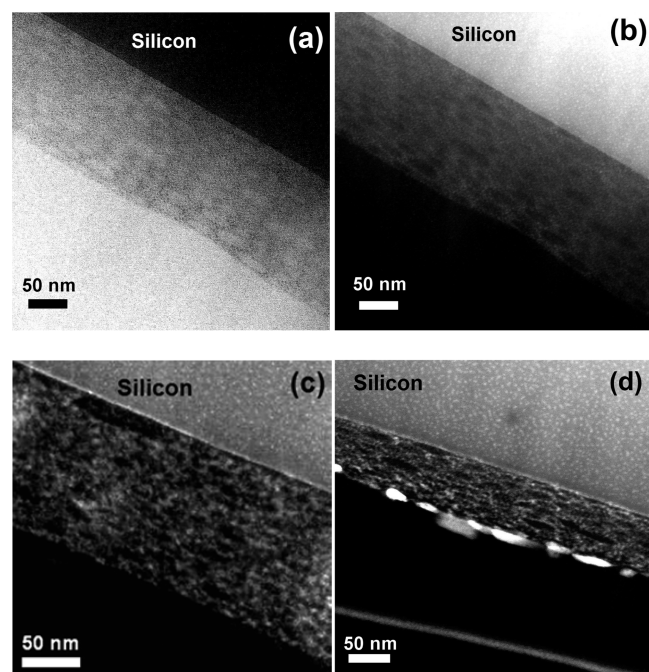
Figure 4. Cross-sectional TEM micrographs of (a) CV-600-N_2 (bright field), (b) CV-600-N_2 (dark field), (c) CV-800-N_2 (dark field), and (d) CV-800-Ar (dark field) illustrating the porous structure of these films. (d) Note the apparent segregation of vanadia to the film surface on calcination in Ar.

consistent with the surface structure obtained from AFM (Figure 2c). The asymmetric pore dimensions arise due to enhanced contraction through the thickness of the inorganic film. The ratio of semimajor to semiminor axes (~2.4) of these pores compares favorably with the change in d-spacing (9.2%) from AFM and thickness contraction (64%) from ellipsometry, from which one would predict an asymmetry ratio of 1.9. Similar pore anisotropy has been reported previously for surfactant-templated inorganic silica[46] and mesoporous carbon thin films,[47] yet the contraction is generally considered to be

unidirectional. From the bright-field image, there are small (~2 nm) dark spots that are attributed to the vanadia due to its large Z. The dark-field imaging (Figure 4b) illustrates small bright spots of similar sizes (~2 ± 1 nm), providing confirmation that these features are due to vanadia.

Upon increasing the calcination temperature to 800 °C, the ordered porous structure deteriorates with significant pore shrinkage (dark spots in the dark-field image), as shown in Figure 4c. The average diameter of the pores along the semimajor axis is estimated to be 15 ± 4 nm. At the same time, isolated vanadia nanoparticles (bright white spots, 3.5 ± 1.5 nm) are mostly dispersed in the film; this increase in size of vanadia nanoparticles with increasing temperature is consistent with modest coarsening of the nanoparticles. The ordering of this porous system is quite poor and the multiple length scales associated with the vanadia nanoparticles in the wall matrix are consistent with the GISAXS data for CV-800-N_2 (Figure 3d). Additionally, there is apparently some aggregation of the vanadia into polycrystalline structures that are on the order of 100 nm in isolated regions in the film (Figure S5 in the Supporting Information).

In the case of CV-800-Ar, significantly larger vanadia particles are observed and these appear to segregate to the free surface of the thin film (Figure 4d). This segregation of vanadia at the film surface helps to explain the disordered surface morphology observed from AFM for CV-600-Ar and CV-800-Ar (Figure 2). As the initial cast films are identical for the two calcination environments, this segregation of vanadia must occur during the calcination. In comparing CV-800-N_2 (Figure 4c) and CV-800-Ar (Figure 4d), the thickness of the film is significantly less for CV-800-Ar, which suggests loss of carbon. If the carbon is preferentially removed from the surface, this would effectively concentrate the remaining vanadia, which would explain the apparent surface segregation. Interestingly, CV-800-Ar also exhibits ellipsoidal pores (dark spots) of highly variable size within the film. The overall mesostructure is slightly altered by distortion from film contraction on calcination. One additional change is the decrease in wall thickness that accompanies the transformation of resol to carbon. This effect is likely exasperated by the carbothermal reduction that leads to further carbon loss and ultimately loss of structure.
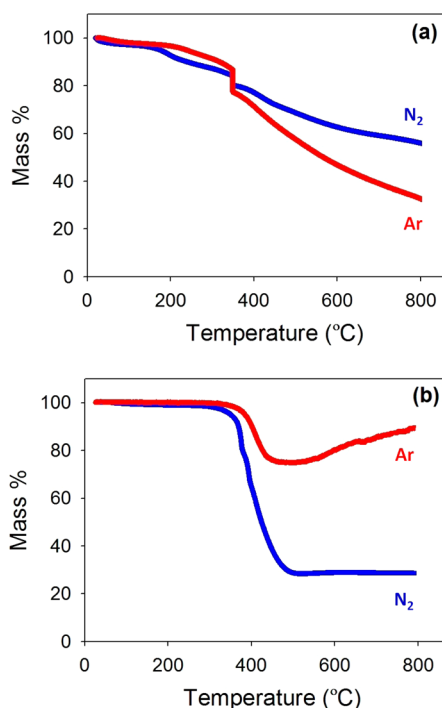
To further investigate the porous structure of the films calcined in N_2, Figure 5 illustrates the adsorption−desorption isotherms using ellipsometric porosimetry (EP) to elucidate the porosity and pore size distribution of these mesostructured films.[37] Figure 5a illustrates that the CV-600-N_2 film exhibits a type-IV isotherm with a H_1-type hysteresis loop. The sharp rise in the adsorption isotherm in the range ($0.7 < p/p_0 < 0.8$) corresponds to capillary condensation in the mesopores. The Lorentz−Lorenz effective medium approximation (EMA) is
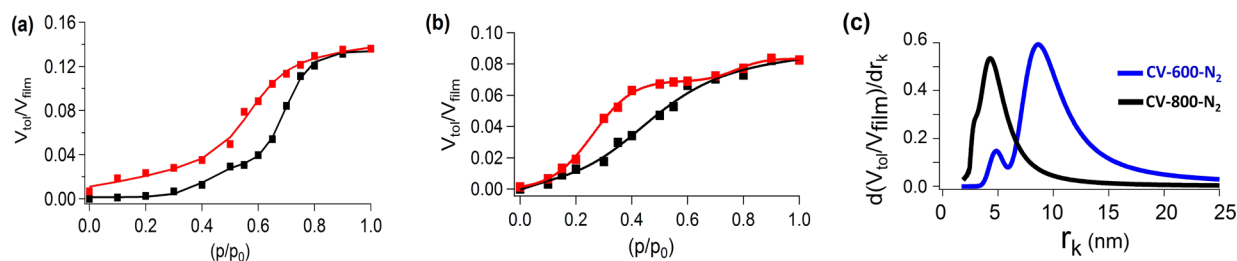
Figure 5. Toluene adsorption (black) and desorption (red) isotherms for (a) CV-600-N_2 and (b) CV-800-N_2. (c) Pore size distribution for CV-600-N_2 and CV-800-N_2 calculated from the adsorption isotherms by using the Kelvin equation.

used to convert the refractive index into volume fraction of adsorbed toluene.[48] Assuming all of the pores are filled by the adsorbed toluene, the porosity is estimated to be 13.6% for CV-600-N$_2$ and 8.5% for CV-800-N$_2$ (Figure 5b). This porosity estimate assumes a uniform porosity through the film, but prior work with mesoporous carbon has suggested that the surface is less porous.[49] The refractive index of optically opaque films is strongly weighed toward the film surface, so these reported porosities are a lower limit. Figure 5c illustrates the pore size distribution for these films. CV-600-N$_2$ exhibits a bimodal pore size distribution with the primary peak centered around r_k ~9.5 nm and a minor peak centered around 5 nm. This compares well with the AFM image for CV-600-N$_2$ (Figure 2c), which suggested a spherical pore diameter of approximately 20 nm ($r_{pore,AFM}$ ~ 10 nm). Increasing the calcination temperature reduces the Kelvin radius to an average r_k of approximately 5 nm (Figure 5c). A minor pore size in the bimodal distribution is again observed, but decreased to around 2 nm. The shrinkage of both pore sizes is consistent between the minor and major component of the pore size distribution.

To more clearly understand the dependence of the morphological differences of the vanadium oxide composites on the calcination environment, we examined the calcination process in greater detail. Figure 6a illustrates the TGA traces for simulated calcination to 800 °C in both N$_2$ and Ar atmospheres using dried and crushed powders of thermopolymerized resol–vanadia sols with an identical initial composition as that of the templated thin films in the absence of the OBO copolymer template. The same heating conditions are utilized in the TGA
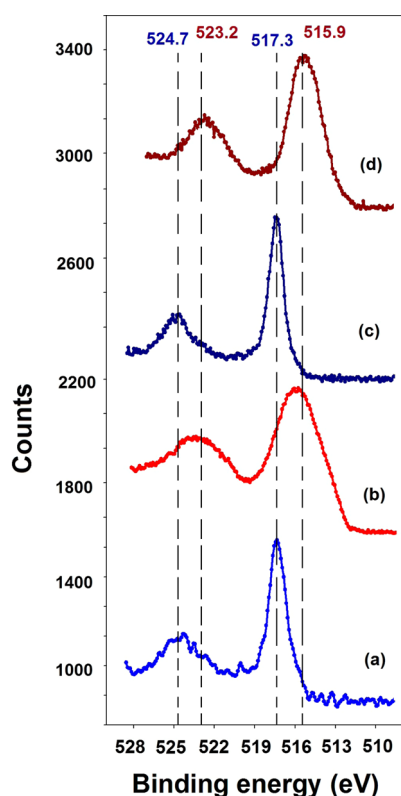
as the calcining conditions used in the tube furnace, which results in the observed mass loss at 350 °C due to the hold at this temperature. There is a clear difference in the mass loss between the two environments. At temperatures below 350 °C, the mass loss in Ar is slightly less than the mass loss under N$_2$. However, upon holding these powders at 350 °C, the loss in Ar begins to exceed that in N$_2$ with the difference in mass loss increasing as temperature increases. The carbon–vanadium oxide residue is 56 wt % at 800 °C when processed in N$_2$ (CV-800-N$_2$), whereas calcination in argon yields only 32 wt % residue on heating to 800 °C (CV-800-Ar). This additional mass loss in Ar is likely due to carbothermal reduction of the vanadium oxide. In N$_2$, there is a possibility for the incorporation of N to form vanadium oxynitrides, although this typically does not occur at temperatures less than 1500 °C.[50]

To both determine the vanadium oxide content and to assess whether any carbothermal reduction occurred within these calcined composites, the above residues from thermogravimetry were heated in air at 10 °C/min to remove the residual carbon by oxidation, as shown in Figure 5b. Both residues exhibit almost no changes until 360 °C, above which the residue obtained from carbonization in N$_2$ (CV-800-N$_2$) begins to lose mass. The residue obtained in Ar remains thermally stable until 410 °C.

Careful inspection of the TGA traces associated with the above residues indicates significant differences in their shapes. The TGA trace for the sample fabricated under N$_2$ follows a typical sigmoid associated with the oxidative removal of the carbon in air, to yield 28 wt % residual vanadium oxide (Figure 6b). On the other hand, the mass of the residue obtained in Ar reaches a minimum near 500 °C on heating CV-800-Ar in air. At temperatures greater than 500 °C, the apparent sample mass increases, which is attributed to the oxidation of vanadium to the V^{5+} oxidation state.[51−53] The continuous increase in mass suggests that the oxidation of vanadium to the V^{5+} oxidation state remains incomplete after heating to 800 °C. This behavior is in contrast to the CV-800-N$_2$ residue, which lacks any apparent increase in mass; this suggests that the vanadium oxide is predominately V$_2$O$_5$ when calcined in N$_2$. These TGA traces indicate that CV-800-N$_2$ is initially 72 wt % carbon, whereas CV-800-Ar is estimated to contain only approximately 25 wt % carbon.

The significantly lower carbon content for CV-800-Ar along with its apparent lower oxidation state for the vanadium suggests that the Ar environment promotes carbothermal reduction of vanadium oxide. In the process of carbothermal reduction, the released oxygen lowers the carbon content in the composite through formation of CO(g) and CO$_2$(g). These differences in the carbon yield between the Ar and N$_2$ environments are likely responsible for the significant differences in morphology observed in the templated films as shown in Figure 2, especially at the higher temperatures.

To directly demonstrate the differences in the oxidation state of vanadium between those calcined in Ar and N$_2$, we performed high resolution XPS scans associated with the vanadium V 2p peaks for the calcined carbon–vanadium oxide thin films, as shown in Figure 7. The films calcined in N$_2$ exhibit a distinct V 2p$_{3/2}$ peak at 517.3 eV and a V 2p$_{1/2}$ peak at 524.7 eV; these peak locations are attributed to vanadium oxide in the V^{5+} oxidation state.[54,55] This occurrence of the V^{5+} oxidation state also agrees well with the TGA data for the sample calcined in N$_2$, wherein no increase in mass is observed

Figure 6. (a) Mass evolution during calcination of thermopolymerized resol–vanadium oxide composites using Ar and N$_2$ as determined by TGA. There is significantly greater residue at 800 °C using N$_2$. (b) Determination of the vanadia content by heating in air of CV-800-N$_2$ (28 wt %); heating of CV-800-Ar residue (red) in air demonstrates that the vanadium is not in its highest oxidation state, as there is an increase in mass on heating above 500 °C, indicative of vanadium oxidation.

Figure 7. High resolution XPS profiles for V 2p peaks for resol-assisted triconstituent thin films calcined under different environments for (a) CV-600-N_2, (b) CV-600-Ar, (c) CV-800-N_2, and (d) CV-800-Ar. N_2 calcined films contain predominately V^{5+} and Ar calcined films contain predominately V^{4+}.

at elevated temperatures upon heating in air. The V 2p peak positions are independent of temperature for calcination in N_2. Resolving the V $2p_{3/2}$ peak indicates ~97% of the vanadium oxide population is present as V^{5+} with less than 3% vanadium to be present in lower V^{4+} oxidation state (515.8 eV). One alternative reason for the increased stability of the nanostructure in N_2 is the formation of an oxynitride[50] that is less reactive for the oxidation of carbon. A high resolution scan for N 1s illustrates a small peak at 397.2 eV (Figure S6, Supporting Information). The elemental composition of nitrogen is calculated to be 1.8% on the basis of these XPS measurements. Thus, a small amount of nitrogen is incorporated within the vanadium oxide−carbon composite during the calcination process; however, the absence of vanadium nitride V $2p_{3/2}$ peak at 513.3 eV[56,57] suggests that negligible vanadium nitride is formed at 800 °C under N_2 calcination. The predominance of vanadium oxide, not oxynitride or nitride, was further confirmed by FTIR (Figure S7, Supporting Information).

Interestingly, there is a shift in the V $2p_{3/2}$ peak toward a lower binding energy (515.9 eV) for the films calcined in Ar at 600 and 800 °C (Figure 7), corresponding to vanadium oxide in the V^{4+} oxidation state.[54,55] The V $2p_{1/2}$ peak is also at a lower binding energy of 523.2 eV, as compared to that for N_2 calcined thin films at the equivalent temperature. After the V $2p_{3/2}$ peak is resolved, CV-600-Ar and CV-800-Ar indicate approximately 94% vanadium to be present as V^{4+}, with 6% vanadium in an even lower oxidation state. This decreased oxidation state of the vanadium oxide in the argon calcined thin films confirms that the Ar environment promotes carbothermal reduction at much lower temperatures when compared to

nitrogen. Similar conclusions can be drawn based on the FTIR spectra (Figure S7, Supporting Information) of the calcined carbon−vanadia composites.

To attempt to explain the difference in morphology based on the calcination environment, prior work associated with the carbothermal reduction of vanadia has been examined. Nitride formation actually promotes the formation of the vanadium carbide at lower temperatures than analogous carbothermal reduction in Ar,[58] but these focused on temperatures in excess of 1000 °C. The partial carbothermal reduction of lithium vanadates at 585 °C has been reported for lithium ion battery electrodes, but the impact of the atmosphere was not discussed.[59] Thus, this difference in carbothermal reduction of vanadia in Ar and N_2 at low temperatures appears to be relatively unexplored.

For the data presented herein, one additional difference between the Ar and N_2 is the oxygen content, which is <1 ppm and <5 ppm, respectively. To understand if this residual oxygen is responsible for the significant difference in the carbon yield and resultant morphology, the calcination of the vanadium oxide-cross-linked resol is examined in ultrapure N_2 (<0.5 ppm of O_2). Based on the TGA traces, calcining the composite under ultrapure nitrogen provides carbon−vanadia residue of 58 wt %, whereas a 56 wt % yield is obtained using nitrogen atmosphere with <5 ppm of O_2 (Figure S8a, Supporting Information). The corresponding vanadium oxide contents are 26 and 28 wt % (Figure S8b, Supporting Information). This indicates that limited difference in O_2 content is not responsible for the differences observed. Thus, we attribute these differences in the carbothermal reduction of vanadia at temperatures less than 800 °C to the formation of a small amount of oxynitride when processed using N_2.

The carbothermal reduction of carbon−vanadia composite thin films leads to loss of templated mesostructure on argon calcining. Hence, the standard protocol of argon calcinations used in the CASH method is not appropriate for templating mesoporous vanadium oxide. However, the N_2 calcination process, in the presence of resol, provides an alternate route to obtain templated mesoporous carbon−vanadium oxide composites. This resol-assisted triconstituent assembly ideally should provide a strategy to develop a wide range of mesoporous metal oxides by removal of carbon matrix. However, removal of the carbon from CV-x-N_2 leads to loss of the ordered mesoporous structure (Figure S9, Supporting Information). This is likely due to the high carbon content (72 wt %) in the composite, but lower carbon content leads to loss of the ordered mesostructure in N_2.

One issue with vanadium oxide as the electroactive material in energy storage devices is its inherently low electrical conductivity.[25] This resol-assisted synthesis provides carbon yields that should endow these materials with enhanced electrical conductivities in order to overcome vanadia limitations for potential electrochemical applications. Interestingly, despite the large differences in carbon yields, the electrical conductivities of samples with a given calcination temperature are almost unaffected by the calcining atmosphere (Figure S10 in the Supporting Information). At 600 °C, the electrical conductivity is relatively low (0.6 ± 0.2 S/cm), but this increases significantly on calcining at 800 °C to 8.2 ± 0.4 S/cm and 14 ± 4 S/cm for CV-800-N_2 and CV-800-Ar, respectively. This conductivity is approximately 3 orders of magnitude greater than that of pure vanadium oxide,[60] yet the conductivity

is slightly less than that reported for mesoporous carbon thin films processed at 800 °C (~20 S/cm).[47]

To test the impact of the improved electrical conductivity and templated porosity on the electrochemical energy storage capabilities for the vanadium oxide, cyclic voltammetry in 1 M $Na_2SO_4(aq)$ electrolyte was used to determine the capacitance of the mesoporous carbon−vanadium oxide composite (CV-800-N_2) as shown in Figure 8a. At a slow scan rate of 2 mV/s, a
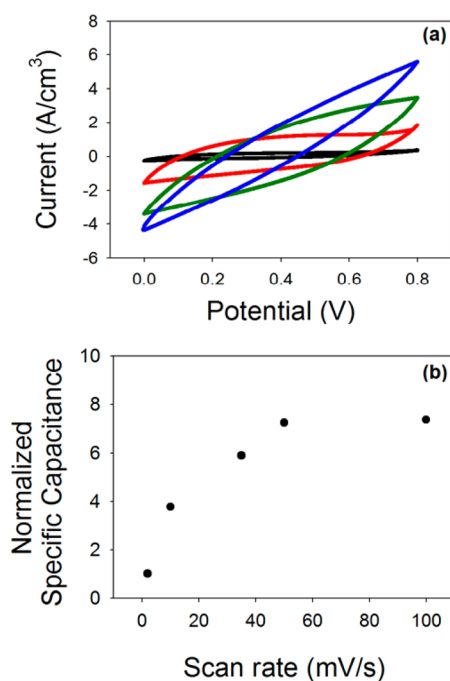
Figure 8. (a) Cyclic voltammetry curves for CV-800-N_2 at scan rates of 2 mV/s (black), 10 mV/s (red), 50 mV/s (green), and 100 mV/s (blue). (b) Normalized specific capacitance of OBO-templated porous CV-800-N_2 (relative to nonporous, nontemplated carbon−vanadium oxide film) at different scan rates.

specific capacitance of 136.1 F/cm^3 is obtained for the templated film. This specific capacitance decreases significantly to 43.4 F/cm^3 at 50 mV/s and 17.4 F/cm^3 at 100 mV/s with increasing scan rates.

The effect of porosity on the charge storage capabilities of carbon−vanadium oxide thin film electrodes is shown in Figure 8b by comparison of the specific capacitance of the templated CV-800-N_2 to the nontemplated analog. At the slowest scan rate examined (2 mV/s), the specific capacitance of the nontemplated composite film (133.6 F/cm^3) is nearly identical to that of the templated film. This illustrates that the primary charge storage mechanism is likely pseudocapacitance through the redox reactions with vanadium oxide.[61] As these reactions are not diffusion limited under these conditions, the capacitance of these films is nearly identical at slower scan rates (2 mV/s). However, at faster scan rates, the impact of porosity becomes apparent. As the scan rate increases, the difference between the templated and nontemplated film increases due to the decreased diffusion length associated with the porous structure.[62] When the scan rate reaches 50 mV/s, the specific capacitance obtained from CV-800-N_2 is almost 7.25 times greater than that of the nonporous composite. This difference does not continue to grow as the rate is further increased to 100 mV/s. The porous architecture allows improved access of electrolyte ions to the vanadium

oxide, but at sufficiently large rates (~50 mV/s), the charge insertion becomes diffusion limited, and thus no additional improvements in relative performance are observed.

CONCLUSION

In this work, we demonstrated the importance of processing conditions in the formation and stabilization of porous carbon−vanadium oxide thin films. Using the standard CASH method, carbothermal reduction of vanadia occurs in the presence of argon, leading to loss of the block copolymer-templated porous architecture. However, using a resol-assisted approach and by calcining under a nitrogen atmosphere, ordered porous carbon−vanadium oxide thin films were obtained at temperatures up to 800 °C. Generally, the nature of the inert calcining environments is not considered when synthesizing such mesoporous materials. However, this study illustrates the crucial role played by the calcining environment in the development of surfactant-templated metal oxides to the action of the limited incorporation of N into the vanadium oxide framework, which prevents its carbothermal reduction. The mesoporous carbon−vanadium oxide composites calcined in nitrogen at 800 °C are found to have electrical conductivity as high as 8.2 S/cm, which is around 3 orders of magnitude higher than that of pure vanadium oxide.

ASSOCIATED CONTENT

⑤ Supporting Information

TGA curves for PEO-PBD-PEO template and thermopolymerized resol, FTIR spectra of the mesoporous materials, ascast AFM images of resol-assisted triconstituent assembled thin films and films calcined in air, ellipsometric film thickness measurements, exponential decay function, TEM micrographs of samples prepared from scratched films, XPS survey scan for CV-800-N_2, TGA trace, and electrical conductivity measurements. This material is available free of charge via the Internet at http://pubs.acs.org.

AUTHOR INFORMATION

Corresponding Author

*B. D. Vogt. E-mail: vogt@uakron.edu.

Author Contributions

The paper was written through contributions of all authors. All authors have given approval to the final version of the paper.

Notes

The authors declare no competing financial interest.

ACKNOWLEDGMENTS

■ REFERENCES

(1) Schüth, F. Non-Siliceous Mesostructured and Mesoporous Materials. *Chem. Mater.* **2001**, *13*, 3184−3195.

(2) Deng, Y.; Wei, J.; Sun, Z.; Zhao, D. Large-Pore Ordered Mesoporous Materials Templated from Non-Pluronic Amphiphilic Block Copolymers. *Chem. Soc. Rev.* **2013**, *42*, 4054−4070.

(3) Sanchez, C.; Boissière, C.; Grosso, D.; Laberty, C.; Nicole, L. Design, Synthesis, and Properties of Inorganic and Hybrid Thin Films Having Periodically Organized Nanoporosity. *Chem. Mater.* **2008**, *20*, 682−737.

(4) Brezesinski, T.; Wang, J.; Senter, R.; Brezesinski, K.; Dunn, B.; Tolbert, S. H. On the Correlation between Mechanical Flexibility, Nanoscale Structure, and Charge Storage in Periodic Mesoporous CeO_2 Thin Films. *ACS Nano* **2010**, *4*, 967−977.

(5) Kresge, C. T.; Leonowicz, M. E.; Roth, W. J.; Vartuli, J. C.; Beck, J. S. Ordered Mesoporous Molecular Sieves Synthesized by a Liquid-Crystal Template Mechanism. *Nature* **1992**, *359*, 710−712.

(6) Shirokura, N.; Nakajima, K.; Nakabayashi, A.; Lu, D.; Hara, M.; Domen, K.; Tatsumi, T.; Kondo, J. N. Synthesis of Crystallized Mesoporous Transition Metal Oxides by Silicone Treatment of the Oxide Precursor. *Chem. Commun.* **2006**, 2188−2190.

(7) Bass, J. D.; Grosso, D.; Boissiere, C.; Sanchez, C. Pyrolysis, Crystallization, and Sintering of Mesostructured Titania Thin Films Assessed by in Situ Thermal Ellipsometry. *J. Am. Chem. Soc.* **2008**, *130*, 7882−7897.

(8) Grosso, D.; Boissière, C.; Smarsly, B.; Brezesinski, T.; Pinna, N.; Albouy, P. A.; Amenitsch, H.; Antonietti, M.; Sanchez, C. Periodically Ordered Nanoscale Islands and Mesoporous Films Composed of Nanocrystalline Multimetallic Oxides. *Nat. Mater.* **2004**, *3*, 787−792.

(9) Yang, P.; Zhao, D.; Margolese, D. I.; Chmelka, B. F.; Stucky, G. D. Block Copolymer Templating Syntheses of Mesoporous Metal Oxides with Large Ordering Lengths and Semicrystalline Framework. *Chem. Mater.* **1999**, *11*, 2813−2826.

(10) Nedelcu, M.; Lee, J.; Crossland, E. J. W.; Warren, S. C.; Orilall, M. C.; Guldin, S.; Hüttner, S.; Ducati, C.; Eder, D.; Wiesner, U.; Steiner, U. Block Copolymer Directed Synthesis of Mesoporous TiO_2 for Dye-Sensitized Solar Cells. *Soft Matter* **2009**, *5*, 134−139.

(11) Ryoo, R.; Joo, S. H.; Jun, S. Synthesis of Highly Ordered Carbon Molecular Sieves via Template-Mediated Structural Transformation. *J. Phys. Chem. B* **1999**, *103*, 7743−7746.

(12) Rumplecker, A.; Kleitz, F.; Salabas, E.; Schüth, F. Hard Templating Pathways for the Synthesis of Nanostructured Porous Co_3O_4. *Chem. Mater.* **2007**, *19*, 485−496.

(13) Roggenbuck, J.; Tiemann, M. Ordered Mesoporous Magnesium Oxide with High Thermal Stability Synthesized by Exotemplating Using CMK-3 Carbon. *J. Am. Chem. Soc.* **2005**, *127*, 1096−1097.

(14) Zhang, Z.; Zhou, Y.; Zhang, Y.; Zhou, S.; Shi, J.; Kong, J.; Zhang, S. Well-Crystallized Mesoporous TiO_2 Shells for Enhanced Photocatalytic Activity: Prepared by Carbon Coating and Silica-Protected Calcination. *Dalton Trans.* **2013**, *42*, 5004−5012.

(15) Lee, J.; Orilall, M. C.; Warren, S. C.; Kamperman, M.; DiSalvo, F. J.; Wiesner, U. Direct Access to Thermally Stable and Highly Crystalline Mesoporous Transition-Metal Oxides with Uniform Pores. *Nat. Mater.* **2008**, *7*, 222−228.

(16) Hwang, J.; Kim, J.; Ramasamy, E.; Choi, W.; Lee, J. Easy Access to Highly Crystalline Mesoporous Transition-Metal Oxides with Controllable Uniform Large Pores by Using Block Copolymers Synthesized via Atom Transfer Radical Polymerization. *Microporous Mesoporous Mater.* **2011**, *143*, 149−156.

(17) Ostomel, T. A.; Stucky, G. D. Free-Standing Mesoporous Titania Films with Anatase Nanocrystallites Synthesized at 80°C. *Chem. Commun.* **2004**, 1016−1017.

(18) Zhang, D.; Wen, M.; Zhang, P.; Zhu, J.; Li, G.; Li, H. Microwave-Induced Synthesis of Porous Single-Crystal-like TiO_2 with Excellent Lithium Storage Properties. *Langmuir* **2012**, *28*, 4543−4547.

(19) Kohn, P.; Pathak, S.; Stefik, M.; Ducati, C.; Wiesner, U.; Steiner, U.; Guldin, S. Low Temperature Crystallisation of Mesoporous TiO_2. *Nanoscale* **2013**, *5*, 10518−10524.

(20) Ye, Y.; Jo, C.; Jeong, I.; Lee, J. Functional Mesoporous Materials for Energy Applications: Solar Cells, Fuel Cells, and Batteries. *Nanoscale* **2013**, *5*, 4584−4605.

(21) Ishii, Y.; Kanamori, Y.; Kawashita, T.; Mukhopadhyay, I.; Kawasaki, S. Mesoporous Carbon−Titania Nanocomposites for High-Power Li-Ion Battery Anode Material. *J. Phys. Chem. Solids* **2010**, *71*, 511−514.

(22) Jiang, H.; Ma, J.; Li, C. Mesoporous Carbon Incorporated Metal Oxide Nanomaterials as Supercapacitor Electrodes. *Adv. Mater.* **2012**, *24*, 4197−4202.

(23) Ji, X.; Herle, P. S.; Rho, Y.; Nazar, L. F. Carbon/MoO_2 Composite Based on Porous Semi-Graphitized Nanorod Assemblies from In Situ Reaction of Tri-Block Polymers. *Chem. Mater.* **2007**, *19*, 374−383.

(24) Dai, M.; Song, L.; LaBelle, J. T.; Vogt, B. D. Ordered Mesoporous Carbon Composite Films Containing Cobalt Oxide and Vanadia for Electrochemical Applications. *Chem. Mater.* **2011**, *23*, 2869−2878.

(25) Muster, B. J.; Kim, G. T.; Krstic, V.; Park, J. G.; Park, Y. W.; Roth, S. Electrical Transport Through Individual Vanadium Pentoxide Nanowires. *Adv. Mater.* **2000**, *12*, 420−424.

(26) Engstrom, A. M.; Doyle, F. M. Exploring the Cycle Behavior of Electrodeposited Vanadium Oxide Electrochemical Capacitor Electrodes in Various Aqueous Environments. *J. Power Sources* **2013**, *228*, 120−131.

(27) Liu, P.; Moudrakovski, I. L.; Liu, J.; Sayari, A. Mesostructured Vanadium Oxide Containing. *Chem. Mater.* **1997**, *9*, 2513−2520.

(28) Luca, V.; MacLachlan, D. J.; Hook, J. M.; Withers, R. Synthesis and Characterization of Mesostructured Vanadium Oxide. *Chem. Mater.* **1995**, *7*, 2220−2223.

(29) Crepaldi, E. L.; Grosso, D.; Soler-Illia, G. J.; de, A. A.; Albouy, P.; Amenitsch, H.; Sanchez, C. Formation and Stabilization of Mesostructured Vanadium-Oxo-based Hybrid Thin Films. *Chem. Mater.* **2002**, *14*, 3316−3325.

(30) Caes, S.; Arrebola, J. C.; Krins, N.; Eloy, P.; Gaigneaux, E. M.; Henrist, C.; Cloots, R.; Vertruyen, B. Mesoporous Lithium Vanadium Oxide as a Thin Film Electrode for Lithium-Ion Batteries: Comparison between Direct Synthesis of LiV_2O_5 and Electrochemical Lithium Intercalation in V_2O_5. *J. Mater. Chem. A* **2014**, *2*, 5809−5815.

(31) Huang, C.-H.; Gu, D.; Zhao, D.; Doong, R.-A. Direct Synthesis of Controllable Microstructures of Thermally Stable and Ordered Mesoporous Crystalline Titanium Oxides and Carbide/Carbon Composites. *Chem. Mater.* **2010**, *22*, 1760−1767.

(32) Olivetti, E. A.; Kim, J. H.; Sadoway, D. R.; Asatekin, A.; Mayes, A. M. Sol−Gel Synthesis of Vanadium Oxide within a Block Copolymer Matrix. *Chem. Mater.* **2006**, *18*, 2828−2833.

(33) Schmitt, A. L.; Mahanthappa, M. K. Polydispersity-Driven Shift in the Lamellar Mesophase Composition Window of PEO-PB-PEO Triblock Copolymers. *Soft Matter* **2012**, *8*, 2294.

(34) Schmitt, A. L.; Repollet-Pedrosa, M. H.; Mahanthappa, M. K. Polydispersity-Driven Block Copolymer Amphiphile Self-Assembly into Prolate-Spheroid Micelles. *ACS Macro Lett.* **2012**, *1*, 300−304.

(35) Meng, Y.; Gu, D.; Zhang, F.; Shi, Y.; Cheng, L.; Feng, D.; Wu, Z.; Chen, Z.; Wan, Y.; Stein, A.; Zhao, D. A Family of Highly Ordered Mesoporous Polymer Resin and Carbon Structures from Organic−Organic Self-Assembly. *Chem. Mater.* **2006**, *18*, 4447−4464.

(36) Stafford, C. M.; Roskov, K. E.; Epps, T. H.; Fasolka, M. J. Generating Thickness Gradients of Thin Polymer Films via Flow Coating. *Rev. Sci. Instrum.* **2006**, *77*, 023908.

19297

dx.doi.org/10.1021/am505307t | *ACS Appl. Mater. Interfaces* 2014, 6, 19288−19298

(37) Hidalgo, N.; López-López, C.; Lozano, G.; Calvo, M. E.; Míguez, H. Characterization of Mesoporous Thin Films by Specular Reflectance Porosimetry. *Langmuir* **2012**, *28*, 13777−13782.

(38) Langford, R. M.; Clinton, C. In Situ Lift-out Using a FIB-SEM System. *Micron* **2004**, *35*, 607−611.

(39) Smith, F. M. Measurement of Sheet Resisitivities with the Four-Point Probe. *Bell Syst. Technol. J.* **1958**, *37*, 711−718.

(40) Eckhardt, B.; Ortel, E.; Bernsmeier, D.; Polte, J.; Strasser, P.; Vainio, U.; Emmerling, F.; Kraehnert, R. Micelle-Templated Oxides and Carbonates of Zinc, Cobalt, and Aluminum and a Generalized Strategy for Their Synthesis. *Chem. Mater.* **2013**, *25*, 2749−2758.

(41) Olivetti, E. A.; Avery, K. C.; Taniguchi, I.; Sadoway, D. R.; Mayes, A. M. Electrochemical Characterization of Vanadium Oxide Nanostructured Electrode. *J. Electrochem. Soc.* **2008**, *155*, A488.

(42) Pauli, S. A.; Herger, R.; Willmott, P. R.; Donev, E. U.; Suh, J. Y.; Haglund, R. F. X-Ray Diffraction Studies of the Growth of Vanadium Dioxide Nanoparticles. *J. Appl. Phys.* **2007**, *102*, 073527.

(43) Urade, V. N.; Wei, T.; Tate, M. P.; Kowalski, J. D.; Hillhouse, H. W. Nanofabrication of Double-Gyroid Thin Films. *Chem. Mater.* **2007**, *19*, 768−777.

(44) Tanaka, S.; Katayama, Y.; Tate, M. P.; Hillhouse, H. W.; Miyake, Y. Fabrication of Continuous Mesoporous Carbon Films with Face-Centered Orthorhombic Symmetry through a Soft Templating Pathway. *J. Mater. Chem.* **2007**, *17*, 3639.

(45) Gao, W.; Wan, Y.; Dou, Y.; Zhao, D. Synthesis of Partially Graphitic Ordered Mesoporous Carbons with High Surface Areas. *Adv. Energy Mater.* **2011**, *1*, 115−123.

(46) Boissiere, C.; Grosso, D.; Lepoutre, S.; Nicole, L.; Bruneau, A. B.; Sanchez, C. Porosity and Mechanical Properties of Mesoporous Thin Films Assessed by Environmental Ellipsometric Porosimetry. *Langmuir* **2005**, *21*, 12362−12371.

(47) Li, X.; Larson, A. B.; Jiang, L.; Song, L.; Prichard, T.; Chawla, N.; Vogt, B. D. Evolution of Mechanical, Optical and Electrical Properties of Self-Assembled Mesostructured Phenolic Resins during Carbonization. *Microporous Mesoporous Mater.* **2011**, *138*, 86−93.

(48) Vayer, M.; Nguyen, T. H.; Grosso, D.; Boissiere, C.; Hillmyer, M. A.; Sinturel, C. Characterization of Nanoporous Polystyrene Thin Films by Environmental Ellipsometric Porosimetry. *Macromolecules* **2011**, *44*, 8892−8897.

(49) Song, L.; Feng, D.; Campbell, C. G.; Gu, D.; Forster, A. M.; Yager, K. G.; Fredin, N.; Lee, H.-J.; Jones, R. L.; Zhao, D.; Vogt, B. D. Robust Conductive Mesoporous Carbon−Silica Composite Films with Highly Ordered and Oriented Orthorhombic Structures from Triblock-Copolymer Template Co-Assembly. *J. Mater. Chem.* **2010**, *20*, 1691−1702.

(50) Tripathy, P. K.; Sehra, J. C.; Kulkarni, A. V. On the Carbonitrothermic Reduction of Vanadium Pentoxide. *J. Mater. Chem.* **2001**, *11*, 691−695.

(51) Zhou, X.; Wu, G.; Gao, G.; Cui, C.; Yang, H.; Shen, J.; Zhou, B.; Zhang, Z. The Synthesis, Characterization and Electrochemical Properties of Multi-Wall Carbon Nanotube-Induced Vanadium Oxide Nanosheet Composite as a Novel Cathode Material for Lithium Ion Batteries. *Electrochim. Acta* **2012**, *74*, 32−38.

(52) Quites, F. J.; Pastore, H. O. Hydrothermal Synthesis of Nanocrystalline VO_2 from Poly(diallyldimethylammonium) Chloride and V_2O_5. *Mater. Res. Bull.* **2010**, *45*, 892−896.

(53) Sediri, F.; Gharbi, N. From Crystalline V_2O_5 to Nanostructured Vanadium Oxides Using Aromatic Amines as Templates. *J. Phys. Chem. Solids* **2007**, *68*, 1821−1829.

(54) Silversmit, G.; Depla, D.; Poelman, H.; Marin, G. B.; De Gryse, R. An XPS Study on the Surface Reduction of V_2O_5(001) Induced by Ar^+ Ion Bombardment. *Surf. Sci.* **2006**, *600*, 3512−3517.

(55) Silversmit, G.; Depla, D.; Poelman, H.; Marin, G. B.; De Gryse, R. Determination of the V2p XPS Binding Energies for Different Vanadium Oxidation States (V^{5+} to V^{0+}). *J. Electron Spectrosc. Relat. Phenom.* **2004**, *135*, 167−175.

(56) Glaser, A.; Surnev, S.; Netzer, F. P.; Fateh, N.; Fontalvo, G. A.; Mitterer, C. Oxidation of Vanadium Nitride and Titanium Nitride Coatings. *Surf. Sci.* **2007**, *601*, 1153−1159.

(57) Choi, D.; Blomgren, G. E.; Kumta, P. N. Fast and Reversible Surface Redox Reaction in Nanocrystalline Vanadium Nitride Supercapacitors. *Adv. Mater.* **2006**, *18*, 1178−1182.

(58) Eick, B. M.; Youngblood, J. P. Carbothermal Reduction of Metal-Oxide Powders by Synthetic Pitch to Carbide and Nitride Ceramics. *J. Mater. Sci.* **2009**, *44*, 1159−1171.

(59) Tran, N.; Bramnik, K. G.; Hibst, H.; Prölß, J.; Mronga, N.; Holzapfel, M.; Scheifele, W.; Novák, P. Spray-Drying Synthesis and Electrochemical Performance of Lithium Vanadates as Positive Electrode Materials for Lithium Batteries. *J. Electrochem. Soc.* **2008**, *155*, A384.

(60) Li, M.; Sun, G.; Yin, P.; Ruan, C.; Ai, K. Controlling the Formation of Rodlike V_2O_5 Nanocrystals on Reduced Graphene Oxide for High-Performance Supercapacitors. *ACS Appl. Mater. Interfaces* **2013**, *5*, 11462−11470.

(61) Augustyn, V.; Simon, P.; Dunn, B. Pseudocapacitive Oxide Materials for High-Rate Electrochemical Energy Storage. *Energy Environ. Sci.* **2014**, *7*, 1597.

(62) Matsui, T.; Tanaka, S.; Miyake, Y. Correlation between the Capacitor Performance and Pore Structure of Ordered Mesoporous Carbons. *Adv. Powder Technol.* **2013**, *24*, 737−742.

19298

dx.doi.org/10.1021/am505307t | *ACS Appl. Mater. Interfaces* 2014, 6, 19288−19298